Extracting phase information on continuum-continuum couplings

Anne Harth,[1,*] Nicolas Douguet,[2] Klaus Bartschat,[3] Robert Moshammer,[1] and Thomas Pfeifer[1]
[1]*Max Planck Institute for Nuclear Physics, 69117 Heidelberg, Germany*
[2]*Department of Physics, University of Central Florida, Orlando 32789, USA*
[3]*Department of Physics and Astronomy, Drake University, Des Moines, Iowa 50311, USA*

(Received 21 May 2018; revised manuscript received 30 October 2018; published 8 February 2019)

In measurements of relative phases in photoionization processes, the contribution of continuum-continuum (CC) couplings to the atomic (Wigner) phases, corresponding to attosecond time delays, is currently accounted for only by theoretical models. Here, we introduce a measurement scheme that is sensitive to phase differences of CC transitions after photoionization in the presence of an optical field. The method allows us to separate CC transitions from the ionization process and can help in testing existing theoretical models. It is based on a multicolor interferometer, similar to the RABBITT (reconstruction of attosecond beating by interference of two-photon transitions) method. The key idea involves the comparison of two measurements with different orders of CC transitions. The scheme is illustrated by an *ab initio* calculation on atomic hydrogen.

DOI: 10.1103/PhysRevA.99.023410

Attosecond time delays of photoionization processes are currently observed by superimposing high-frequency (e.g., extreme ultraviolet, XUV) photons with an optical field [1–3]. Two experimental methods have been developed to measure these processes: the streaking approach, where an isolated attosecond pulse triggers the photoionization [4,5], and the reconstruction of attosecond beating by interference of two-photon transitions (RABBITT) method [6,7], which uses an attosecond pulse train (APT). In both methods, the optical field probes the ionization step by interacting with the photoelectron. This interaction causes the observable of interest, the photoionization time delay, to be shifted by an additional time delay, which is called Coulomb-laser coupling in the streaking method [8] or continuum-continuum (CC) time delay in RABBITT [9]. The additional shift is often large enough to have a non-negligible effect on the measurement. At present, it is estimated solely based on calculations.

Taking the RABBITT method as example, photoelectron signals at energy ϵ, also called sidebands (SB_ϵ), are generated with amplitudes that oscillate depending on the time delay τ between the optical field ω_p and the XUV field. The measured oscillation contains a phase $\Delta\phi_\epsilon$ according to

$$\mathrm{SB}_\epsilon \propto \cos(-2\,\omega_p\tau + \Delta\phi_\epsilon). \tag{1}$$

$\Delta\phi_\epsilon$ can be expressed by three contributions [3,10]:

$$\Delta\phi_\epsilon \approx \Delta\phi_{\mathrm{xuv},\epsilon} + \Delta\phi_{\mathrm{W},\epsilon} + \Delta\phi_{\mathrm{CC},\epsilon}. \tag{2}$$

The first contribution, $\Delta\phi_{\mathrm{xuv}}$, carries the spectral dispersion of the pulses in the APT and can be used to estimate the average XUV pulse duration [7,11]. The second contribution, $\Delta\phi_{\mathrm{W}}$, is related to the Eisenbud-Wigner-Smith (EWS) time delay [12–15], i.e., the photoionization time delay. $\Delta\phi_{\mathrm{CC}}$ is the additional phase shift leading to the CC time delay [3,16].

A direct measurement approach for the latter phase shift that could confirm theoretical models would be desirable. In this paper, we describe a scheme that makes it possible to experimentally access information on this phase shift. The method allows us to isolate the interaction of an optical field with a continuum electron, from the ionization step and experimental conditions. The key idea is to compare two RABBITT-like measurements in which the contributions of the chirp of the XUV attosecond pulses and the photoionization time delay cancel each other. Unless stated otherwise, atomic units are used throughout this manuscript.

We first illustrate the method based on the RABBITT technique by means of a simplified perturbative description. Consider an APT produced by the process of high-order harmonic generation (HHG), e.g., [17], where the intense driving field is not the fundamental (as in a traditional RABBITT experiment) but the second harmonic ($2\omega_L$) of a multicycle laser with frequency ω_L, e.g., [18]. In such an XUV spectrum, the separation of the high-order harmonic peaks (HH) is twice the driving frequency, i.e., $4\,\omega_L$. Now it is possible to choose either the fundamental angular frequency ω_L ("red") or the second harmonic $2\,\omega_L$ ("blue") as the probe field with angular frequency ω_p.

As illustrated in Fig. 1 (blue), the RABBITT method is based on the quantum interference of two different pathways leading to the same photoelectron signal at energy ϵ, the sideband signal (SB_ϵ). In one quantum path, a HH of odd order q, HH(q), generates a photoelectron by absorption of one photon of the probe field with angular frequency $\omega_p = 2\,\omega_L$. For the other path, a photoelectron generated by HH($q+2$) emits a probe photon.

The final SB photoelectron signal at state ψ_ϵ, generated by the "blue" probe field, can be estimated as $\mathrm{SB}_\epsilon^{(\mathrm{blue})} = |M_{\epsilon g}^{(2,e)} + M_{\epsilon g}^{(2,a)}|^2$ by two matrix elements describing the interfering paths, $M_{\epsilon g}^{(2,e)}$ and $M_{\epsilon g}^{(2,a)}$, which can be expressed using second-order perturbation theory. The index "ϵg" indicates that the transition is between the ground state ψ_g and the

*anne.harth@mpi-hd.mpg.de

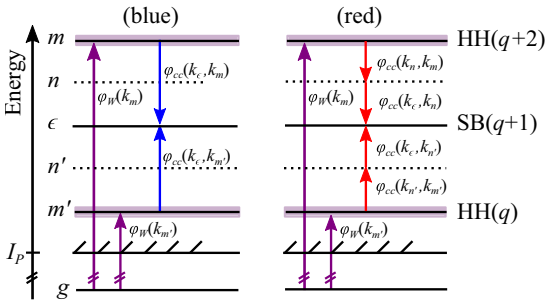

FIG. 1. Schematic representation of the multicolor RABBITT method: The purple arrows describe the one-photon ionization process by the high-order harmonics HH(q) and HH($q+2$); I_P labels the ionization threshold. Sidebands (SB) are generated either by a two-photon process with the second harmonic frequency (case "blue") or by a three-photon process with the fundamental (case "red"). See text for details.

final state ψ_ϵ, "2" that it is a two-photon matrix element, and "e/a" that it describes the path that emits/ or absorbs a probe photon.

The matrix elements depend on the XUV field harmonics $E_q(t) = |E_q|\, e^{i\varphi_q} e^{iq2\omega_L t}$ and on the delayed probe field $E_{\omega_p}(t) = |E_{\omega_p}|\, e^{i\varphi_\omega} e^{i\omega_p t}$ with $\varphi_\omega = \omega_p \tau$. The harmonic phase is denoted as φ_q. Based on the asymptotic approximation [9], and assuming the same intermediate angular momentum of the states ψ_m and $\psi_{m'}$, the phase of the matrix elements can be written as [see Eq. (25) in [9]]

$$\arg\left[M^{(2,e)}_{\epsilon g}\right] = \varphi_{q+2} - \varphi_\omega + \varphi_{\rm W}(k_m) + \varphi_{\rm CC}(k_\epsilon, k_m) + \phi_C, \tag{3}$$

$$\arg\left[M^{(2,a)}_{\epsilon g}\right] = \varphi_q + \varphi_\omega + \varphi_{\rm W}(k_{m'}) + \varphi_{\rm CC}(k_\epsilon, k_{m'}) + \phi_C. \tag{4}$$

Here the labels of the states correspond to Fig. 1. The phase "$\varphi_{\rm W}(k_m)$" is the scattering phase of the intermediate state ψ_m with wave number k_m; "$\varphi_{\rm CC}(k_\epsilon, k_m)$" is the phase associated with CC transitions from state ψ_m to state ψ_ϵ; and ϕ_C is a constant phase geometrical [9].

The SB oscillation depends on the time delay τ:

$$\begin{aligned}{\rm SB}^{\rm (blue)}_\epsilon &\propto \cos\left(\arg\left[M^{(2,e)}_{\epsilon g}\right] - \arg\left[M^{(2,a)}_{\epsilon g}\right]\right)\\ &\propto \cos\left(-4\,\omega_L\tau + \Delta\phi_{{\rm xuv},\epsilon} + \Delta\phi_{{\rm W},\epsilon} + \Delta\phi^{(1)}_{{\rm CC},\epsilon}\right).\end{aligned} \tag{5}$$

As seen from the above equation, $\Delta\phi_{{\rm xuv},\epsilon} = (\varphi_{q+2} - \varphi_q)$ carries the group delay dispersion of the attosecond pulses in the APT. If the pulses in the APT are Fourier limited (FL), the phase φ_q is the same for all harmonics, and $\Delta\phi_{{\rm xuv},\epsilon} = 0$. It also follows that $\Delta\phi_{{\rm W},\epsilon} = \varphi_{\rm W}(k_m) - \varphi_{\rm W}(k_{m'})$ is the phase difference between the two one-photon ionization steps from the ground state ψ_g to the continuum states ψ_m and $\psi_{m'}$. Finally,

$$\Delta\phi^{(1)}_{{\rm CC},\epsilon}(2\,\omega_L) = \varphi_{\rm CC}(k_\epsilon, k_m) - \varphi_{\rm CC}(k_\epsilon, k_{m'}). \tag{6}$$

The superscript "(1)" (and later "(2)") indicates that in order to reach the sideband, one (two) photon(s) of the probe frequency is (are) needed.

Choosing now the fundamental field ω_L as probe, the quantum-path interference involves two three-photon transitions, $M^{(3,e)}_{\epsilon g}$ and $M^{(3,a)}_{\epsilon g}$, cf. Fig. 1 (red), including two CC transitions [16] instead of one:

$$\arg\left[M^{(3,e)}_{\epsilon g}\right] = \varphi_{q+2} - \varphi_\omega + \varphi_{\rm W}(k_m) + \varphi_{\rm CC}(k_\epsilon, k_n) + \varphi_{\rm CC}(k_n, k_m) + \phi_C, \tag{7}$$

$$\arg\left[M^{(3,a)}_{\epsilon g}\right] = \varphi_q + \varphi_\omega + \varphi_{\rm W}(k_{m'}) + \varphi_{\rm CC}(k_\epsilon, k_{n'}) + \varphi_{\rm CC}(k_{n'}, k_{m'}) + \phi_C. \tag{8}$$

The SB signal can be written as

$$\begin{aligned}{\rm SB}^{\rm (red)}_\epsilon &\propto \cos\left(\arg\left[M^{(3,e)}_{\epsilon g}\right] - \arg\left[M^{(3,a)}_{\epsilon g}\right]\right)\\ &\propto \cos\left(-4\,\omega_L\tau + \Delta\phi_{{\rm xuv},\epsilon} + \Delta\phi_{{\rm W},\epsilon} + \Delta\phi^{(2)}_{{\rm CC},\epsilon}\right),\end{aligned} \tag{9}$$

with

$$\Delta\phi^{(2)}_{{\rm CC},\epsilon}(\omega_L) = \varphi_{\rm CC}(k_\epsilon, k_n) + \varphi_{\rm CC}(k_n, k_m) - \varphi_{\rm CC}(k_\epsilon, k_{n'}) - \varphi_{\rm CC}(k_{n'}, k_{m'}). \tag{10}$$

Therefore, the total phase shift for both cases, blue and red, can be written as

$$\Delta\phi^{\rm (blue)}_\epsilon \propto \Delta\phi_{{\rm xuv},\epsilon} + \Delta\phi_{{\rm W},\epsilon} + \Delta\phi^{(1)}_{{\rm CC},\epsilon}(2\,\omega_L), \tag{11}$$

$$\Delta\phi^{\rm (red)}_\epsilon \propto \underbrace{\Delta\phi_{{\rm xuv},\epsilon} + \Delta\phi_{{\rm W},\epsilon}}_{\text{same for both}} + \underbrace{\Delta\phi^{(2)}_{{\rm CC},\epsilon}(\omega_L)}_{\text{different}}. \tag{12}$$

Since the ionization step and the XUV spectrum are the same, the first two contributions, i.e., the chirp of the XUV pulses and the EWS time-delay contribution, are identical for both cases. Only the last contribution, $\Delta\phi_{\rm CC}$, differs. In this lowest order of perturbation theory and within the asymptotic approximation [9], therefore, CC contributions can be isolated from the ionization step.

Experimentally, one would first perform a RABBITT measurement with a probe field $\omega_p = 2\,\omega_L$ and thereby retrieve the phase $\Delta\phi^{\rm (blue)}_\epsilon$ of all sidebands at energy ϵ. In a second step, the experiment would be repeated with a probe frequency $\omega_p = \omega_L$. Within the asymptotic approximation [9], the phase difference $\Delta\phi^{\rm (blue)}_\epsilon - \Delta\phi^{\rm (red)}_\epsilon$ is then a direct measurement of the phase difference of the CC contributions

$$\begin{aligned}&\Delta\phi^{(1)}_{{\rm CC},\epsilon}(2\,\omega_L) - \Delta\phi^{(2)}_{{\rm CC},\epsilon}(\omega_L)\\ &= \varphi_{\rm CC}(k_\epsilon, k_m) - \varphi_{\rm CC}(k_\epsilon, k_{m'}) - \varphi_{\rm CC}(k_\epsilon, k_n)\\ &\quad - \varphi_{\rm CC}(k_n, k_m) + \varphi_{\rm CC}(k_\epsilon, k_{n'}) + \varphi_{\rm CC}(k_{n'}, k_{m'}).\end{aligned} \tag{13}$$

We now illustrate the general ideas of the method by simulating a multicolor RABBITT experiment in an artificial system. The initial coarse-grained model consists of a few discrete energy levels, which include the ground state and a few continuum states. The reduction of continuum states is sufficient for demonstrating the key idea, as the perturbative interactions with the comb-like XUV spectrum and a constant laser frequency can be approximated by a few effective states.

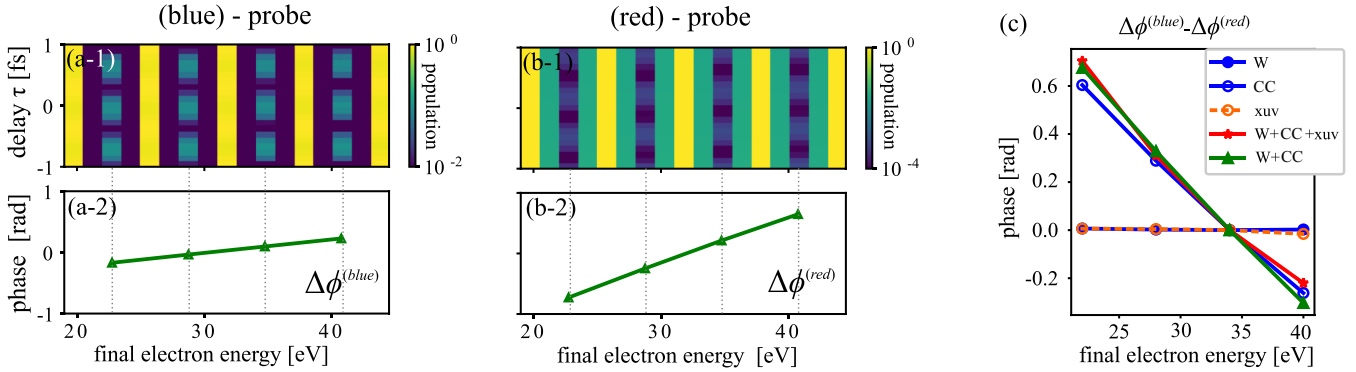

FIG. 2. Simulation of RABBITT traces in an artificial few-level system using probe fields with frequency $2\,\omega_L$ (a) or ω_L (b). (a-1) and (b-1): Population of the continuum states as a function of the photoelectron energy and the delay between the APT and the probe field. (a-2) and (b-2): Phase information $\Delta\phi^{(\mathrm{blue})}$ and $\Delta\phi^{(\mathrm{red})}$ retrieved from the RABBITT data in (a-1) and (b-1). The phase difference $\Delta\phi^{(\mathrm{blue})} - \Delta\phi^{(\mathrm{red})}$ is shown in (c) for different sets of couplings (see text). Parameters for this simulation: $\omega_L = 1.5$ eV; harmonics separation: $4\,\omega_L$; intensity of the APT: 10^{-4} W/cm^2; intensity of the probe field: 10^7 W/cm^2; modulus of all couplings: $|\mu_{ij}| = 5.95$ atomic units; CC coupling: $\varphi_{\mathrm{CC}}(k_i, k_j) = -0.5{k_i}^2/2$; EWS contribution: $\varphi_W(k_i) = -0.002{k_i}^2/2$; and XUV chirp: group delay dispersion GDD $= -8.68$ atomic units.

The total wave function is expanded as (i runs over all states, the ground state and continuum states)

$$|\psi(t)\rangle = \sum_i c_i(t)\ |\chi_i\rangle\, e^{-i\omega_i t}, \tag{14}$$

i.e., as a superposition of basis states $|\chi_i\rangle$ that diagonalize the unperturbed atomic Hamiltonian H_0 according to $\langle\chi_i|H_0|\chi_j\rangle = \delta_{ij}\omega_i$. Note that in this description the states can be of arbitrary kind.

The evolution of the complex-valued, time-dependent amplitudes $c_i(t)$ can be calculated by solving the time-dependent Schrödinger equation (TDSE) in the interaction picture

$$i\frac{\partial}{\partial t}\,|\psi(t)\rangle = V(t)\ |\psi(t)\rangle\,, \tag{15}$$

where $V(t)$ is the coupling operator with $\langle\chi_i|V(t)|\chi_j\rangle = \mu_{ij}E(t)$, $\mu_{ii} = 0$, and $E(t)$ as the electric field. Inserting Eq. (14) into (15) yields the coupled differential equations

$$\dot{c}_i(t) = -i\sum_j c_j(t)\mu_{ij}\ e^{-i(\omega_j-\omega_i)t}\ E(t). \tag{16}$$

The indices i and j include the ground state and the continuum states.

The electric field is composed of the APT and the probe field: $E(t) = E_{\mathrm{xuv}}(t) + E_{\omega_p}(t-\tau)$. The XUV and probe-field amplitudes are chosen such that a perturbative treatment is appropriate. Note that the results do not depend on the probe intensity in the perturbative case. The modulus of all possible couplings μ_{ij} between states $|\chi_j\rangle$ and $|\chi_i\rangle$ is set to be the same in this simulation.

Solving the coupled differential equations (16) and varying the delay τ between the two fields yields the population probabilities $P_i \propto |c_i|^2$ of the states, which are associated with the ionization probability in the RABBITT experiment; see Figs. 2(a-1) and 2(b-1) with probe frequencies $2\,\omega_L$ and ω_L, respectively. From the delay-dependent sideband oscillation the RABBITT phase $\Delta\phi_\epsilon$ [cf. Eq. (2)] can be extracted for each sideband. The result is shown in Figs. 2(a-2) and 2(b-2). The phase difference $\Delta\phi^{(\mathrm{blue})} - \Delta\phi^{(\mathrm{red})}$ is plotted in Fig. 2(c).

If all coupling constants are real and the pulses in the APT are FL, the RABBITT phase of both scans is zero and the phase difference $\Delta\phi^{(\mathrm{blue})} - \Delta\phi^{(\mathrm{red})}$ vanishes. If the coupling constants are real and the pulses in the APT are chirped, the RABBITT phases are not zero. The phases are exactly the same (except for a constant), and thus the phase difference $\Delta\phi^{(\mathrm{blue})} - \Delta\phi^{(\mathrm{red})}$ vanishes again. This case is labeled "xuv" in Fig. 2(c).

Next, if the pulses in the APT are FL and the phases of the coupling constants μ_{ig}, which couple the ground state χ_g to the continuum states χ_i, are energy dependent, e.g., $\mu_{ig} = |\mu_{ig}|e^{i\varphi_{\mathrm{W}}(k_i)}$, with φ_{W} being associated with the EWS phase, then the RABBITT phases $\Delta\phi^{(\mathrm{blue/red})}$ exhibit the same phase shift as a function of energy. Thus, the phase difference $\Delta\phi^{(\mathrm{blue})} - \Delta\phi^{(\mathrm{red})}$ vanishes. This case is labeled "W".

Lastly, if the phases of the coupling constants, which describe the coupling only between continuum states, are energy dependent, e.g., $\mu_{ij} = |\mu_{ij}|e^{i\varphi_{\mathrm{CC}}(k_i,k_j)}$ with φ_{CC} being associated with the CC phase, the RABBITT phases $\Delta\phi^{(\mathrm{blue/red})}$ are no longer identical. In this case the phase difference $\Delta\phi^{(\mathrm{blue})} - \Delta\phi^{(\mathrm{red})}$ does not vanish; see the curve labeled "CC" in Fig. 2(c).

For the two RABBITT scans shown in Figs. 2(a) and 2(b), the initial conditions are set with $\varphi_{\mathrm{CC}} \neq 0$ and $\varphi_{\mathrm{W}} \neq 0$ but with FL pulses in the APT. The phase difference is shown in Fig. 2(c) labeled "W+CC". This curve follows the curve "CC", where only the CC phase was considered. The same result holds if the attosecond pulses are chirped, as seen in the curve labeled "W+CC+xuv".

This toy model demonstrates in a very general way that the method of comparing two RABBITT-like measurements performed with two different probe frequencies is sensitive to the coupling between continuum states and isolates them from the coupling between ground and continuum states, as well as from the chirp of the XUV pulses.

We now move to a realistic case, namely, an *ab initio* TDSE calculation for two RABBITT experiments in atomic hydrogen. The problem is treated in full dimensionality. While certain elements of the physics are ignored (such as relativistic and quantum-field effects) and the numerical treatment is

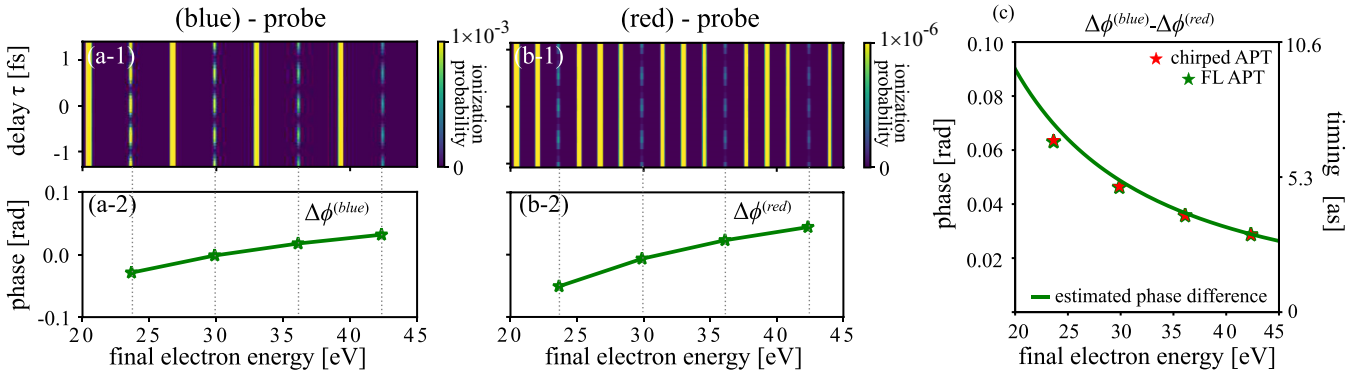

FIG. 3. *Ab initio* TDSE calculation of two RABBITT experiments in atomic hydrogen using probe fields with frequency $2\,\omega_L$ (a) or ω_L (b). (a-1),(b-1) and (a-2),(b-2) are analogs to Fig. 2. The phase difference $\Delta\phi^{(\mathrm{blue})} - \Delta\phi^{(\mathrm{red})}$ is shown in (c). Also shown is the reference curve (green line) based on an analytical approximation for $\Delta\phi_{\mathrm{CC}}$ (see text). The phase can be converted into a time via $(\Delta\phi^{(\mathrm{blue})} - \Delta\phi^{(\mathrm{red})})/(2\omega_p)$, as shown on the right axis in (c). Parameters for this simulation: $\omega_L = 1.5$ eV; harmonics separation: $4\,\omega_L$; intensity of each harmonic field: 10^9 W/cm^2; and intensity of the probe field I_p: 10^{11} W/cm^2. Green stars: Fourier-limited APT; red stars: chirped APT with an attosecond pulse GDD $= -0.8656$ in atomic units.)

carried out on a discretized space-time grid (for details, see [19]), the accuracy of the results can safely be assumed to be better than any remaining uncertainty that could be eliminated in current experimental setups. Furthermore, since both the EWS and the CC contributions can be calculated accurately for atomic hydrogen [8,9], the system is ideally suited to verifying the ideas presented above.

Figures 3(a) and 3(b) show two sets of simulated RABBITT data with the corresponding RABBITT phases, one with a "blue" and one with a "red" probe frequency. The phase difference $\Delta\phi^{(\mathrm{blue})} - \Delta\phi^{(\mathrm{red})}$ is plotted with green stars in Fig. 3(c).

The reference curve (green solid curve) in the same figure is produced by plotting the phase difference given in Eq. (13) with the analytical formula for the CC contribution in hydrogen given in Ref. [9] [Eq. (30)] for the standard RABBITT configuration. This analytical formula is based on an asymptotic approximation for two-photon ATI matrix elements. However, based on the discussion above, the phase difference $\Delta\phi^{(\mathrm{blue})} - \Delta\phi^{(\mathrm{red})}$ includes several CC contributions, cf. Eq. (13).

The data points from the *ab initio* calculation match the reference curve very well. Since the analytical formula in [9] becomes less accurate for energies below 20 eV, we expect deviations for lower energies.

The simulation leading to the green data points was performed with FL attosecond pulses. The red data points in Fig. 3(c) were obtained from a simulation that included an attochirp. Since they lie on top of each other, these results confirm that the method essentially isolates the CC contribution from the XUV pulse shape.

To summarize, since all current attosecond experiments based on the RABBITT or streaking technique depend on calculations of $\Delta\phi_{\mathrm{CC}}$ [8,9,20], measurements can now profile related data in order to examine, e.g., the degree of universality of the expression for $\Delta\phi_{\mathrm{CC}}$ given in [9]. Different combinations of HHG driving frequencies and probe fields are possible, as long as only those data are compared that involve the same one-photon ionization steps. It will most likely first be performed in atomic noble gases, such as argon or neon, using a photoelectron spectrometer.

Furthermore, employing a three-dimensional momentum spectrometer and tailored probe fields, such as circularly polarized light or multicolor fields, continuum couplings involving sublevels with different magnetic quantum numbers can be studied in even more complex targets such as molecules, clusters, or nanoparticles. In the future this approach might be extended to the study of structured continua in order to provide data particularly for CC couplings near the ionization threshold and close to resonances [2,10].

The work of N.D. and K.B. was supported by the United States National Science Foundation under Grants No. PHY-1403245 and No. PHY-1803844. The *ab initio* calculations were performed on SuperMIC at the Center for Computation & Technology at Louisiana State University. Access to SuperMIC was made possible through the XSEDE allocation PHY-090031.

[1] M. Schultze, M. Fieß, N. Karpowicz, J. Gagnon, M. Korbman, M. Hofstetter, S. Neppl, A. L. Cavalieri, Y. Komninos, T. Mercouris, C. A. Nicolaides, R. Pazourek, S. Nagele, J. Feist, J. Burgdörfer, A. M. Azzeer, R. Ernstorfer, R. Kienberger, U. Kleineberg, E. Goulielmakis, F. Krausz, and V. S. Yakovlev, Science **328**, 1658 (2010).

[2] M. Isinger, R. Squibb, D. Busto, S. Zhong, A. Harth, D. Kroon, S. Nandi, C. L. Arnold, M. Miranda, J. M. Dahlström, E. Lindroth, R. Feifel, M. Gisselbrecht, and A. L'Huillier, Science **358**, 893 (2017).

[3] K. Klünder, J. M. Dahlström, M. Gisselbrecht, T. Fordell, M. Swoboda, D. Guénot, P. Johnsson, J. Caillat, J. Mauritsson, A. Maquet, R. Taïeb, and A. L'Huillier, Phys. Rev. Lett. **106**, 143002 (2011).

[4] J. Itatani, F. Quéré, G. L. Yudin, M. Y. Ivanov, F. Krausz, and P. B. Corkum, Phys. Rev. Lett. **88**, 173903 (2002).

[5] M. Kitzler, N. Milosevic, A. Scrinzi, F. Krausz, and T. Brabec, Phys. Rev. Lett. **88**, 173904 (2002).
[6] H. Muller, Appl. Phys. B **74**, S17 (2002).
[7] P. Paul, E. Toma, P. Breger, G. Mullot, F. Augé, P. Balcou, H. Muller, and P. Agostini, Science **292**, 1689 (2001).
[8] S. Nagele, R. Pazourek, J. Feist, K. Doblhoff-Dier, C. Lemell, K. Tőkési, and J. Burgdörfer, J. Phys. B **44**, 081001 (2011).
[9] J. Dahlström, D. Guénot, K. Klünder, M. Gisselbrecht, J. Mauritsson, A. L'Huillier, A. Maquet, and R. Taïeb, Chem. Phys. **414**, 53 (2013).
[10] J. M. Dahlström and E. Lindroth, J. Phys. B **47**, 124012 (2014).
[11] S. Klarsfeld and A. Maquet, Phys. Lett. A **78**, 40 (1980).
[12] L. Eisenbud, Ph.D. thesis, Princeton University, 1948.
[13] E. P. Wigner, Phys. Rev. **98**, 145 (1955).
[14] F. T. Smith, Phys. Rev. **118**, 349 (1960).
[15] H. M. Nussenzveig, Phys. Rev. A **55**, 1012 (1997).
[16] J. M. Dahlström, A. L'Huillier, and A. Maquet, J. Phys. B **45**, 183001 (2012).
[17] M. Ferray, A. L'Huillier, X. F. Li, L. A. Lompre, G. Mainfray, and C. Manus, J. Phys. B **21**, L31 (1988).
[18] E. L. Falcão-Filho, C.-J. Lai, K.-H. Hong, V.-M. Gkortsas, S.-W. Huang, L.-J. Chen, and F. X. Kärtner, Appl. Phys. Lett. **97**, 061107 (2010).
[19] N. Douguet, A. N. Grum-Grzhimailo, E. V. Gryzlova, E. I. Staroselskaya, J. Venzke, and K. Bartschat, Phys. Rev. A **93**, 033402 (2016).
[20] L. A. A. Nikolopoulos, Phys. Rev. A **73**, 043408 (2006).